Chinese Chemical Letters 34 (2023) 107563

Contents lists available at ScienceDirect

Chinese Chemical Letters

journal homepage: www.elsevier.com/locate/cclet

In-situ electro-polymerization of L-tyrosine enables ultrafast, long cycle life for lithium metal battery

Zihao Chu, Sidong Zhuang, Jiahui Lu, Jiabao Li, Chengyin Wang, Tianyi Wang*

College of Chemistry and Chemical Engineering, Yangzhou University, Yangzhou 225002, China

ARTICLE INFO

Article history:
Received 24 April 2022
Accepted 24 May 2022
Available online 27 May 2022

Keywords:
Lithium metal battery
Tyrosine
In situ
Electropolymerization
lithium dendrite

ABSTRACT

The growth of dendrites in the lithium (Li) metal anode hinders the commercialization of lithium metal batteries (LMBs). Electrolyte additives have proved to be an effective way to solve the problem of dendrites and improve the coulombic efficiency. Herein, we propose a strategy of using L-tyrosine (L-Tyr) as an additive to protect the lithium metal anode *in situ*, where L-Tyr can be electropolymerized *in situ* to form an ordered array of nanosheets on the surface of the lithium metal anode to uniformly deposit lithium ions. At the same time, the addition of L-Tyr changed the structure of the solvent in the electrolyte, because the carboxyl group on L-Tyr make DME form hydrogen bonds easily. Besides, the reduction of free DME makes more $TFSI^-$ involved in the formation of the SEI film on the electrode surface, which increases the proportion of LiF in the SEI film. With 2 wt% L-Tyr, Li||Li symmetric cells superior cycle stability in ether electrolytes, Li|Cu cells y improved stability up to 200 cycles with an average CE of 93.1% in ether electrolytes and Li||$Li_4Ti_5O_{12}$ (LTO) demonstrated an excellent cycling capabilitie with 119 mAh/g capacity retention by the 5000th cycle.

In the past fifty years, lithium-ion batteries have made exciting commercial achievements. Although there is still room for improvement in technology, it is increasingly difficult to meet the requirements of people for high energy density. Therefore, the high energy density cell system with lithium metal as the anode rises again due to the highest capacities (3.86 Ah/g) and low redox potential (−3.04 V) of metallic lithium (Li) [1,2]. However, due to the disordered deposition of lithium dendrites and the low coulomb efficiency during the battery cycle, safety problems hinder the commercial development of Li anodes [3–5]. At the same time, metallic Li is quite reactive, resulting in the formation of a solid electrolyte interface (SEI) at the moment of contact with the electrolyte The low mechanical electrolyte interface breaks and regrows under the influence of the volume expansion of Li metal during the plating/stripping process, which greatly consumes the electrolyte and reactive metallic Li, leading to the poor cycle stability and short cycle life [6]. In addition, the fractured SEI film makes the deposition of lithium ions uneven, which strengthens the disordered deposition of lithium dendrites, and increases the risk of cell internal short circuit and safe hidden trouble [7,8].

Metallic Li is quite reactive, resulting in the formation of a solid electrolyte interface (SEI) at the moment of contact with the electrolyte. This accumulation of high resistance layers in liquid organic electrolytes leads to premature death of the battery [9,10]. With the aim of disposing of this challenge, considerable research had focused on the interface stability of lithium metal anode. The SEI film should enable uniform lithium deposition and have high lithium ion mobility. Also, it should have a certain degree of mechanical strength and elasticity to meet the volume expansion of Li metal during the cycle [11–13]. There are three main methods to stabilize Li metal anodes: (1) Construct an *in-situ* high ionic conductivity SEI film (such as LiF, Li_3N, Li_2S) on the Li metal surface [14]. (2) Construct SEI film with high mechanical strength and self-healing [15,16]. (3) The addition of electrolyte additive or modification of electrolyte can boost the formation of stable SEI film on lithium metal anode [17–19]. Among these artificial SEI films, LiF is considered to be an excellent component for passivating negative electrodes owing to the electronic conductivity, larger band gap and higher negative electrode electrochemical stability. The brittleness of the inorganic artificial SEI film makes it easy to break when the huge expansion of volume of the metal Li anode at high current density [20,21]. For organic artificial SEI film, although the mechanical modulus is low, its high elasticity can achieve close contact with the electrode, maintain the stability of lithium metal anode, restrain the disorder deposition of dendrite, improve the cycle performance of cell [22–24].

* Corresponding author.
E-mail address: wangty@yzu.edu.cn (T. Wang).

https://doi.org/10.1016/j.cclet.2022.05.077
1001-8417/

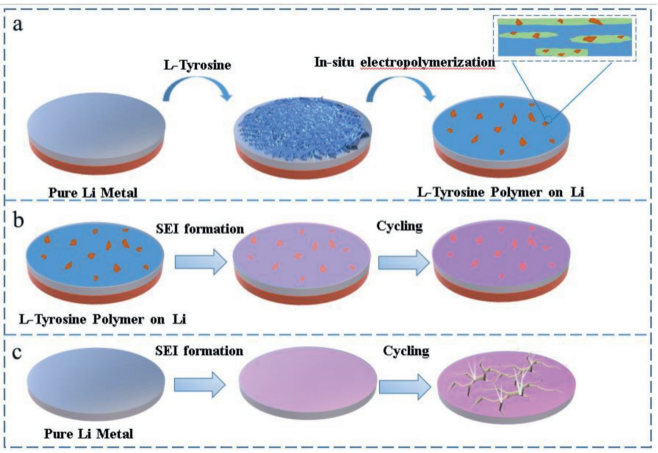

Fig. 1. Schematic illustration of *in-situ* electropolymerization procedure for (a) L-Tyr polymer on Li metal, the Li nucleation and plating process on (b) L-Tyr polymer on Li metal, and (c) Pure Li metal.

Herein, we report a method that uses *in-situ* electropolymerization to suppress disorder deposition of lithium dendrites and maintain stability of SEI film. The phenol group in L-Tyr has electropolymerization ability and can oxidize and polymerize on the surface of the metallic Li to form a film of network polymer. Meanwhile, the carboxyl group in the polymer can be used as a polar group to deposit lithium ions uniformly. Moreover, the carboxyl group on L-Tyr is easy for DME to form hydrogen bonds [25]. During the formation of SEI film, the reduction of free DME makes more $TFSI^-$ move to the electrode surface, thereby increasing the proportion of LiF in the composition of SEI film [26]. As a result, the 1 mol/L LiTFSI in the DOL:DME (1:1) ether electrolyte using L-Tyr as an additive showed excellent cycle life and coulombic efficiency. With 2 wt% Tyr, Li||Li symmetric cells improved electrochemical performance that can maintain a cycle life of more than 800 h under the test conditions of 0.5 mA/cm^2 and 1 mAh/cm^2. Li|Cu cell cycle over 200 cycles with an average CE of 93.1% and Li||$Li_4Ti_5O_{12}$ (LTO) cell has a 6000-cycle life and a discharge capacity of 119 mAh/g by the 5000 cycle.

We use the electropolymerization ability of L-Tyr itself to *in-situ* form a carboxyl-containing polymer protective film on lithium metal to maintain the stability of SEI film and inhibit the disordered deposition of lithium dendrites (Fig. 1). The introduction of Tyr has a high degree of crystallinity as shown by the X-ray diffraction pattern (Fig. S1 in Supporting information). The electropolymerization mechanism of L-Tyr is shown in Fig. 2a. During the cycling, the amino group on L-Tyr is oxidized to lose one H and condense with the carboxylate of another L-Ty to form a polymer of poly-L-Tyr. The Raman spectra was used to analyze the lithium metal anode after cycling (Fig. 2b). The characteristic peak at 510 cm^{-1} are corresponded to the C=O deformation, and the peak at 887 cm^{-1} belonged to the O=C-N deformation. This indicates that the lithium metal shows the formation of a layer of polymer with a peptide chain structure after cycling, which is consistent with the mechanism. In order to further study the polymerized product, we designed a stainless-steel symmetric cell cycle experiment, and analyze the cycled stainless-steel symmetrical cells through the attenuated total reflection flourier transformed infrared spectroscopy (FTIR-ATR). In Fig. 2c, we can see that neither the uncirculated stainless-steel sheet nor the stainless-steel sheet circulating as a cathode has obvious signals. However, the stainless-steel sheet circulating as the anode has a clear infrared spectrum. The peak at 744 and 796 cm^{-1} belonged to *ortho* sub-

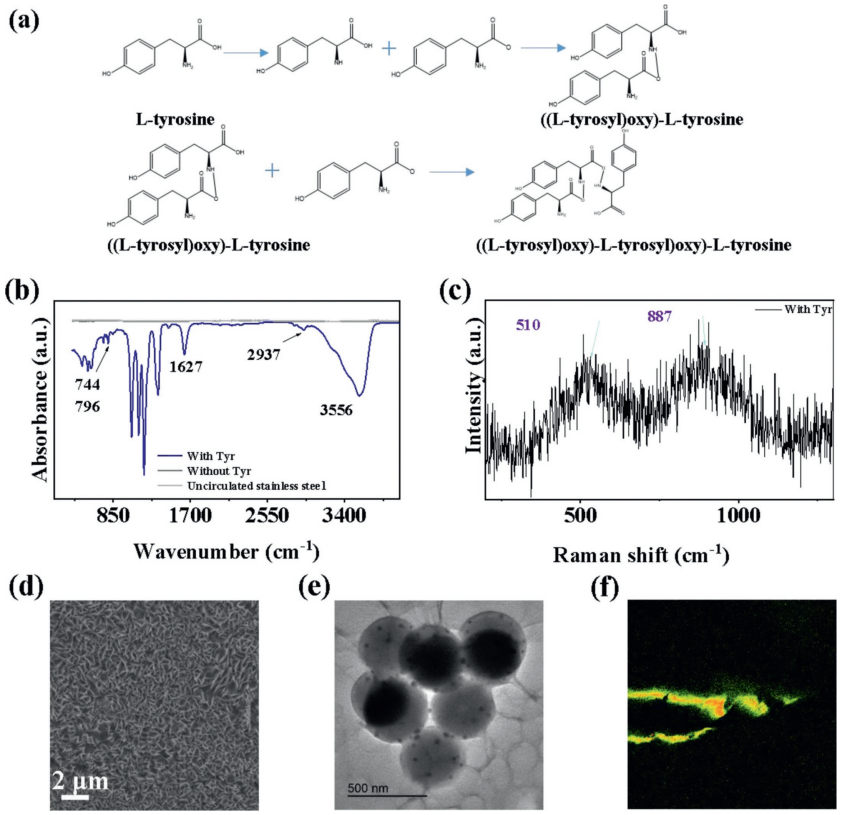

Fig. 2. (a) The mechanism diagram L-Tyr electropolymerization. (b) The Raman spectra for the surface of Li metal anode. (c) FTIR-ATR of stainless-steel symmetric battery. (d) The SEM images of morphology of L-Tyr electropolymerization after 20 cycles. (e) The TEM images of morphology of L-Tyr after electropolymerization. (f) Under ultraviolet light, the fluorescence image of L-Tyr distribution in the damage of Li metal foil.

stitution and *para* substitution. During the electropolymerization, the unpaired electrons in the phenol radical are transferred to the ortho position and the para position through the conjugated structure of the benzene ring. At the same time, the broad peak at 3556 cm^{-1} belonged to the free O-H stretching vibration peak, and the broad peak at 1627 cm^{-1} was assigned to the C=O stretching vibration. The above confirmed that the electropolymerization reaction occurred and the polymer contained carboxyl groups. In order to understand the electropolymerization behavior during electrochemical cycling, we disassembled the Li||Li symmetric cell after cycling and observed lithium metal foil by scanning electron microscope (SEM). The lithium foil after cycling is shown in Fig. S2 (Supporting information). Consistent with the assumption, it can be observed that the L-Tyr formed an ordered array of nanosheets in Fig. 2d. We further characterized the L-Tyr polymeric structure using Transmission Electron Microscope (TEM). It is a structure of spherical sheets stacked together (Fig. 2e). We performed TEM mapping on the cross section of polytyrosine as shown in Fig. S3 (Supporting information). F element is uniformly dispersed on its surface. EDX spectrum shows that polytyrosine has a large amount of F element (Fig. S4 in Supporting information). In addition, protein fluorescence method was used for directly observing the adsorption behavior of L-Tyr on Li metal anode. L-Tyr was stained with fluorescent dye and then dispersed in ether electrolyte. Lithium metal sheets were immersed in the electrolyte and then removed and cleaned with DOL to remove lithium salts and excess L-Tyr. We use the tip of a needle to pierce lithium metal to create defects. As shown in Fig. 2f, the adsorbed L-Tyr was observed under a fluorescence microscope to emit clear fluorescence under ultraviolet light. Especially around the defect of lithium metal, the fluorescence intensity is stronger. This result confirmed that L-Tyr prefers to adsorb at the edges of the damage, such as dendrites or other defects.

With the aim to explore the morphology change of lithium metal after cycling, symmetrical cells were cycled for 30 times. For the cells with L-Tyr additives in the electrolyte, the Li anode formed a dense and uniform deposit (Figs. 3a and b). The SEM images of the cross-sections further confirm the dense structure, which helps to reduce the surface area and stabilize the SEI (Figs. 3d and e). Notably, due to the modulation of the *in-situ* L-Tyr polymer layers, the thicknesses of the two samples differ significantly, and the morphology differences suggest that the L-Tyr polymer film alleviate the disordered deposition of Li dendrites and stabilize the Li anode interface. The SEM images of top-view and cross-section after 30 cycles with the blank electrolyte are shown in Figs. 3c and f. The rough surface and porous structure indicate that the deposited Li is loosely aggregated, which increases the specific surface area and lead to a loss of reactive Li.

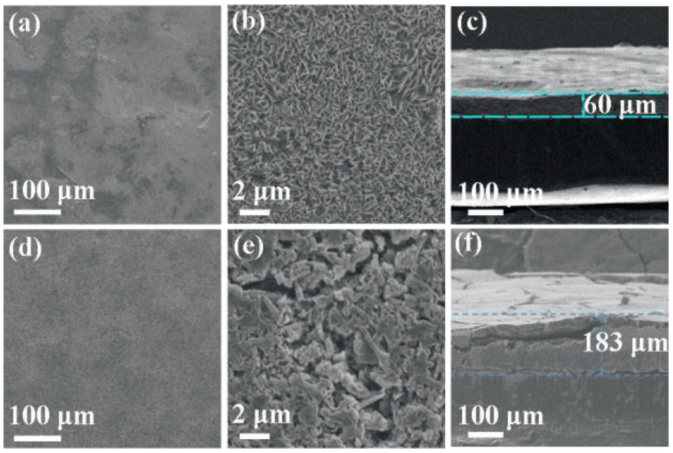

Fig. 3. SEM images of top-view of Li metal anode after 30 cycles (a, b) with the Tyr additive and (d, e) in the blank electrolyte. SEM images of cross-section of Li metal anode cycling in the cells (c) with the Tyr additive and (f) the blank electrolyte.

Furthermore, we tested the Raman spectra of the electrolyte without or with 2 wt% Tyr additive. According to previous reports, the characteristic peaks of free DME are at 360 and 845 cm^{-1} [7]. As shown in Fig. S5 (Supporting information), when solvated with Li, the two pairs of the characteristic peaks of DME upshift to 403 and 872 cm^{-1} in the blank electrolyte. Interestingly, the two pairs of the characteristic peaks of DME upshift to 402 and 875 cm^{-1} in the blank electrolyte with 2 wt% Tyr electrolyte. The $TFSI^-$'s characteristic peak of the blank electrolyte and the blank electrolyte with 2 wt% Tyr electrolyte are 738 and 743 cm^{-1} (Fig. S6 in Supporting information). According to previous work, the characteristic peak of $TFSI^-$ shifted from 738 cm^{-1} to 743 cm^{-1} was caused by the transition of the main form of $TFSI^-$ from free anions to contact ion pairs (CIPs, $TFSI^-$ coordinated with a single Li^+ ion) and aggregates (AGGs, $TFSI^-$ coordinated with two or more Li^+ ions). Based on the above analysis, when adding Tyr additive, the carboxyl group on Tyr is easy to dissociate dimethyl ether to form hydrogen bonds [25]. The formation of hydrogen bonds consumes a large amount of free DME. This makes it easier for most $TFSI^-$ to combine with Li^+ to reach the electrode surface to participate in the formation of SEI film, and the decrease of free DME will reduce the side reactions of solvent and lithium metal.

With aim to further explore the impact of Tyr additives on the composition of SEI film, X-ray photoelectron spectra (XPS) was used to analyze the SEI film composition after circulation [27]. The fitting and separation of XPS peaks are based on the profiles of spectra for a better identification and analysis. The full spectrum of XPS is shown in Fig. S7 (Supporting information). As shown in Fig. 4a and Fig. S8a (Supporting information), with the addition of Tyr additive, the composition of the SEI film on the Li metal surface changed greatly after 10 cycles. The C 1s peaks at 284.4 and 288.8 eV are assigned to C=O and C–O, the apparent increase in the intensity of the C=O peak in the electrolyte with 2 wt% Tyr additive may be due to the carboxyl groups provided by the electropolymerization of Tyr on the Li metal surface. This also con-

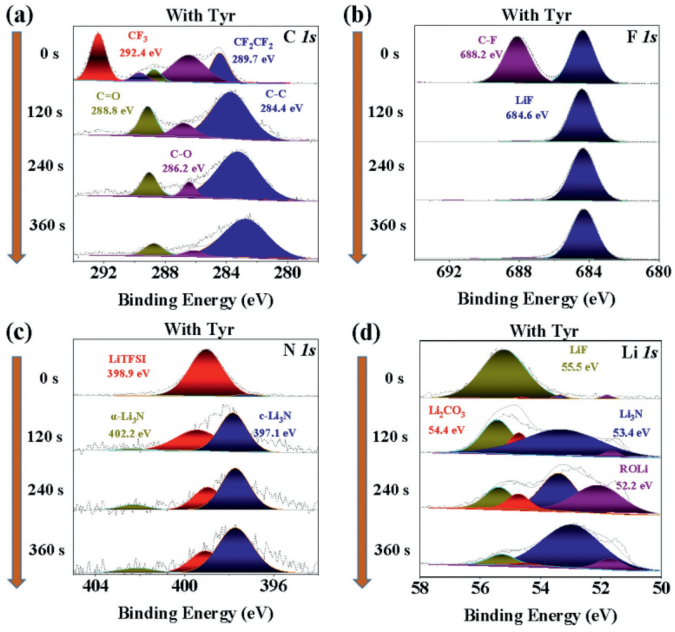

Fig. 4. SEI characterization by XPS. (a) C 1s, (b) F 1s, (c) N 1s and (d) Li 1s spectrum of Tyr-induced SEI.

firmed that Tyr was electropolymerized on the SEI film surface. The new -CF_2CF_2 (289.7 eV) was observed in the electrolyte with the addition of 2 wt% Tyr additive, which may be due to the fact that the addition of Tyr affects the decomposition of $TFSI^-$. Compared with the SEI film composition of two different electrolytes, the F 1s spectrum of the electrolyte with 2 wt% Tyr additive shows a high peak at 684.6 eV (LiF) (Fig. 4b and Fig. S8b in Supporting information). As shown in Fig. 4d, the Li 1s spectrum of the electrolyte with 2 wt% Tyr additive also shows a high peak at 55.5 eV (LiF). It is further confirmed that Tyr additive is beneficial for more $TFSI^-$ to involve in the formation of SEI film on the Li metal anode surface and induce more LiF production. We probed different depths of the SEI film using Ar^+ sputtering. With the increase of sputtering time, the N 1s peak of SEI film formed by electrolyte with Tyr additive was higher than that of SEI film formed by the blank electrolyte (Fig. 4c and Fig. S8d in Supporting information). In particular, α-Li_3N has an additional peak at 402.8 eV in the N 1s spectrum. C-Li_3N exists widely in SEI film formed by ether-based electrolyte containing $LiNO_3$ additive. Compared with C-Li_3N, α-Li_3N is beneficial to the formation of SEI, and has better mechanical stability and higher lithium ion conductivity.

Once the current exceeds the diffusion limit, the increase of lithium migration number and conductivity can alleviate the disorder deposition of lithium dendrites by alleviating the space charge induced electric field between electrode and electrolyte interface. In previous reports, carboxyl groups have been confirmed to be more inclined to combine with 1,2-dimethoxyethane (DME) through hydrogen bonds [28–30]. Thereby reducing the amount of DME coordinated with Li^+ and improving Li-ions mobility. As shown in Fig. 5a, the overpotential values with or without L-Tyr were calculated to be 43.7 and 85.8 mV, indicating L-Tyr polymer layer lower Li nucleation barriers. This may be the result of desolvation at the anode-electrolyte interface. Fig. 5b exhibits the cyclic voltammetry (CV) in the electrolyte with 2 wt% Tyr. Within the potential range of the scan, L-Tyr showed a small oxidation peak around 0.8 V in the first week of polymerization, and the oxidation peak gradually increased as the number of scans increased. Free radicals may be generated during the polymerization process, and the polymerization process may be through free radical polymerization.

The electrochemical stability of electrolyte with Tyr additive is explored by linear sweep voltammetry (LSV). The electrolyte with Tyr additive is stable under the electrochemical window up to 4.7 V (Fig. 5c), which means that the electrolyte containing L-Tyr has a higher oxidation decomposition voltage. In order to further assess the impact of the electrolyte with Tyr additive on the change of polarization voltage. We also compared the polarization voltage changes of lithium-ion symmetric battery with two different electrolytes. With the electrolyte with 2 wt% Tyr additive, stable cycle of Li||Li symmetric cell over 450 h with low over-potential of ~42 mV during the entire cycling under a relatively low current of 0.5 mA/cm^2 with a capacity of 1 mAh/cm^2. In contrast, Li||Li symmetric cells without additive can only operate for ~163 h (Fig. 5d). As shown in Fig. 5e, under 1 mA/cm^2, with the electrolyte with 2 wt% Tyr dditive, Li||Li symmetric cells stably cycles for 400 h with low over-potential of ~73 mV, much longer than without additive (200 h). At 3 mA/cm^2, the electrolyte with 2 wt% Tyr additive is also effective. As shown in Fig. S9 (Supporting information), with the introduction of the Tyr, Li||Li symmetric cells have lower overpotential during the entire cycling. In addition, the cycled Li||Li has lower electrochemical impedance (Fig. S10 in Supporting information). This indicates that the introduction of Try can effectively reduce the interfacial impedance and facilitate the migration of lithium ions. The excellent stability of Li||Li symmetric cells polarization may be attributed to the ordered array of nanosheets generated by Tyr *in-situ* electropolymerization that inhibits dendrite growth.

We assemble the Li|Cu cells to study the electrochemical performance in the electrolyte with 2 wt% Tyr additive. Coulomb efficiency (CE) of Li|Cu is mainly used to characterize the reversibility

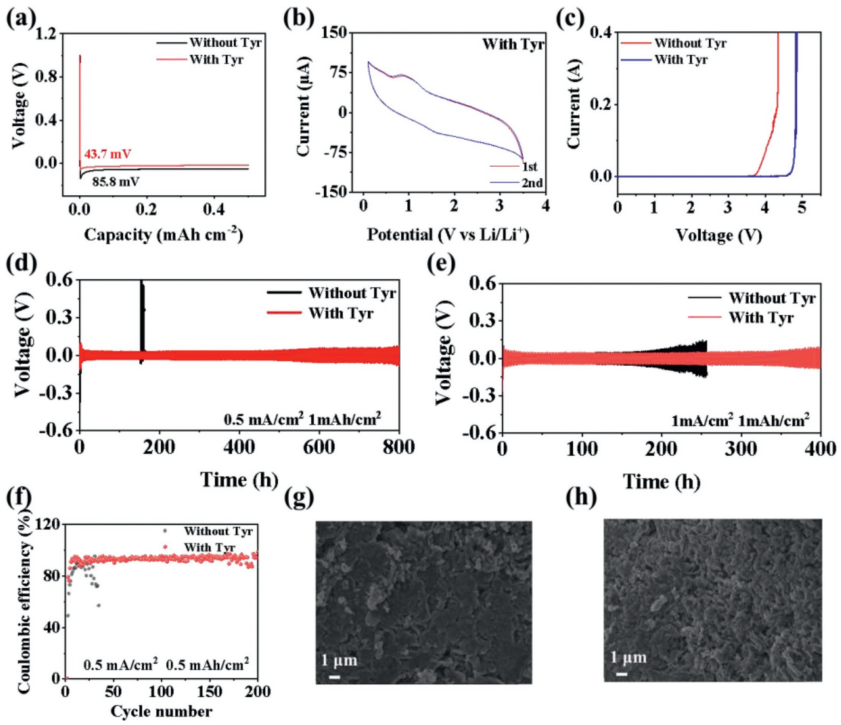

Fig. 5. Cycling capabilities of Li||Li symmetric cells at (a) 0.5 mA/cm^2, (b) 1 mA/cm^2. (c) The cyclic voltamme Tyr of Li||Li symmetric cells with LiTFSI-2 wt% Tyr-DOL/DME. (d) Voltage-specific capacity curve during Li nucleation at 0.05 mA/cm^2 on Cu foil. (e) The linear sweep voltammetry of Li|Cu cells. (f) Cycling capabilities of Li|Cu cells. The SEM images of Cu foil after plating Li (g) with Tyr additive and (h) bank electrolyte.

of electrode plating/stripping. As shown in Fig. 5f, Li|Cu cells with the electrolyte without additive starts to drop only after 16 cycles. In contrast, with the introduction of the Tyr, Li|Cu cells. Li|Cu has stronger electroplating/stripping reversibility. Li|Cu cells increased cycle life to 200 cycles with an average CE of 93.1%. Comparing the specific capacity-voltage Chart of Li|Cu cell with two different electrolytes, we can clearly find that with the introduction of Tyr, the electrochemical performance of Li|Cu cell is improved (Fig S12 in Supporting information). We also tested the coulombic efficiency and cycle life of Cu-Li cells treated with different concentrations of Tyr (Fig S11 in Supporting information). The morphology of Li deposited on Cu foil in two different electrolytes is shown in Figs. 5g and h. After 20 cycles, the appearance of the deposited Li on Cu foil in the electrolyte without additive is rough and loose. Visibly, it can be seen that all the dendrites fall off from the block and form strips of dead Li (Fig. 5h). This also explains the reason for the poor cycle life of Li|Cu cells with the electrolyte without additive. In contrast, the appearance of the electrolyte with 2 wt% Tyr is dense and smooth which corresponds to long cycle life and high CE (Fig. 5g).

To verify the practical application of Tyr additive, we use Li||$Li_4Ti_5O_{12}$ (LTO) cells to evaluate their practical capabilities. The cyclic voltammetry of Li||LTO battery is shown in Fig. S13 (Supporting information). This indicates that the introduction of Tyr did not change the redox reaction of Li||LTO. The electrochemical performance of two different electrolytes in Li LTO battery cell is shown in Fig. 6. The initial coulombic efficiency of the Li||LTO cells with two different electrolytes was very low, resulting in a lower specific discharge capacity at 2 C. The capacity of the Li||LTO cell with the electrolyte without additive quickly dropped from 120 mAh/g to 95 mAh/g. In contrast, with the introduction of the Tyr, the capacity of Li||LTO cell maintained 135 mAh/g after 3000 cycles, showing better performance (Fig. 6a), demonstrating excellent Li metal protection capabilities with minimized parasitic reactions. At 5 C in the Fig. 6b, the LTO cells with the electrolyte with 2 wt% Tyr demonstrate a good cycling performance with 119 mAh/g capacity retention by the 5000th cycle (Fig. 6d), much longer than the electrolyte without additive which quickly dropped from 122 mAh/g to 50 mAh/g. Rate performance was shown in Fig. 6c, the electrolyte with 2 wt% Tyr additive demonstrate reversible capacities of 163.1, 159.1, 154.7, 145.8, 130.1, 117.1 and 95.8 mAh/g at 0.2, 0.3, 0.5, 1, 2, 3 and 5 C which better than that the electrolyte without additive.

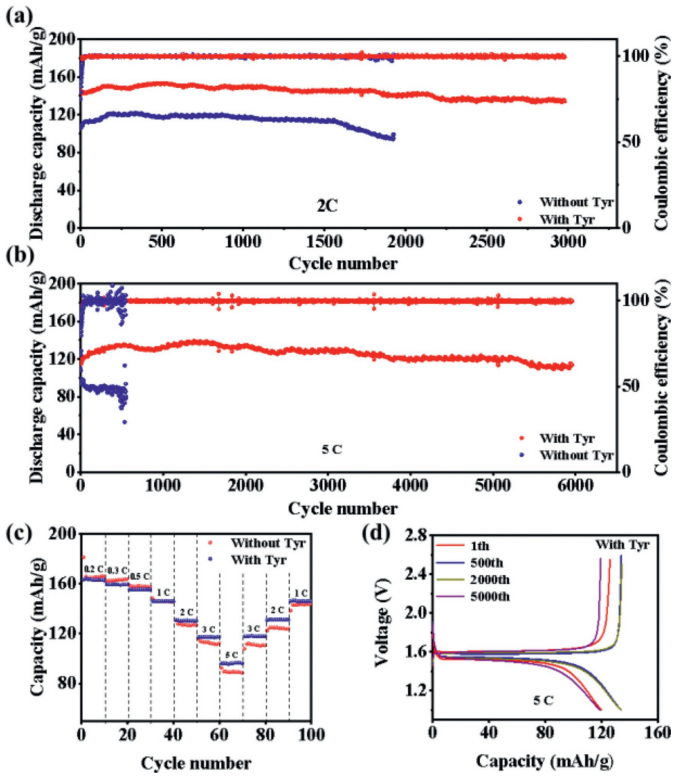

Fig. 6. (a) Cycling capabilities of Li||LTO cells with different electrolyte at 5 C. (b) Cycling capabilities of Li||LTO cells with different electrolyte at 2 C. (c) Rate capabilities of Li||LTO cells from 0.2 C to 5 C. (d) Charge–discharge curves of the first cycle, the 500th cycle, the 2000th cycle and 5000th cycle.

In summary, L-Tyr was introduced as an additive into the conventional DOL/DME electrolyte to solve the problems of relieving disordered deposition of Li dendrite and fragility of SEI film. L-Tyr can be electropolymerized *in situ* on Li anode to form a film of ordered array of nanosheets, which improves the number of lithium ion migration. Furthermore, the carboxyl group on L-Tyr is easy for DME to form hydrogen bonds, reducing the free DME in the electrolyte, making more $TFSI^-$ reach the electrode surface and induce more LiF in the SEI film composition. Therefore, with the introduction of the Tyr, Li||Li symmetric cells stably cycles for 450 h with low over-potential of ~42 mV during the entire cycling under 0.5 mA/cm^2. Li|Cu cells with the electrolyte with 2 wt% Tyr increased cycle life to 200 cycles with an average CE of 93.1%. Moreover, with the introduction of the Tyr, Li||LTO cells achieve long-term stable cycle and high rate performance. Li||LTO demonstrated a good cycling performance with 119 mAh/g capacity retention by the 5000th cycle. This strategy of using natural amino acids as additives provides new ideas for the realization of safe and dendritic-free Li metal anodes.

Declaration of competing interest

The authors declare that they have no known competing financial interests or personal relations hips that could have appeared to influence the work reported in this paper.

Acknowledgments

C.Y. Wang is grateful for the financial supports from the National Natural Science Foundation of China (No. 21978251) and a project funded by the Priority Academic Program Development of Jiangsu Higher Education Institutions. T.Y. Wang is grateful for the financial supports from the National Natural Science Foundation of China (No. 22102141).

Supplementary materials

Supplementary material associated with this article can be found, in the online version, at doi:10.1016/j.cclet.2022.05.077.

References

[1] D.H. Liu, Z. Bai, M. Li, et al., Chem. Soc. Rev. 49 (2020) 5407–5445.
[2] W. Liu, P. Liu, D. Mitlin, Chem. Soc. Rev. 49 (2020) 7284–7300.
[3] Q. Meng, B. Deng, H. Zhang, Energy Storage Mater. 16 (2019) 419–425.
[4] Z. Luo, C. Liu, Y. Tian, et al., Energy Storage Mater. 27 (2020) 124–132.
[5] J. Wang, J. Yang, Q. Xiao, et al., Adv. Funct. Mater. 31 (2021) 2007434.
[6] Y. Gao, Z. Yan, J.L. Gray, et al., Nat. Mater. 18 (2019) 384–389.
[7] S. Wang, J. Qu, F. Wu, K. Yan, C. Zhang, ACS Appl. Mater. Interfaces 12 (2020) 8366–8375.
[8] J. Wu, X. Li, Z. Rao, et al., Nano Energy 72 (2020) 104725.
[9] H.L. Dai, J. Dong, M.J. Wu, G.X. Zhang, S.H. Sun, Angew. Chem. Int. Ed. 60 (2021) 19852–19859.
[10] H.L. Dai, X.X. Gu, J. Dong, et al., Nat. Commun. 11 (2020) 643.
[11] X. Zhang, Y. Yang, Z. Zhou, Chem. Soc. Rev. 49 (2020) 3040–3071.
[12] J.I. Lee, G. Song, S. Cho, D.Y. Han, S. Park, Batter. Supercaps 3 (2020) 790.
[13] X.B. Cheng, R. Zhang, C.Z. Zhao, Q. Zhang, Chem. Rev. 117 (2017) 10403–10407.
[14] S. Ye, L. Wang, F. Liu, et al., Adv. Energy Mater. 10 (2020) 2006247.
[15] S. Yuan, T. Kong, Y. Zhang, et al., Angew. Chem. Int. Ed. 133 (2021) 25828–25842.
[16] Y. Yu, Y. Liu, J. Xie, ACS Appl. Mater. Interfaces 13 (2021) 18–33.

[17] S.J. Tan, W.P. Wang, Y.F. Tian, S. Xin, Y.G. Guo, Adv. Funct. Mater. 31 (2021) 2105253.
[18] X. Zheng, L. Huang, X. Ye, et al., Chem 7 (2021) 2312–2346.
[19] D. Lin, Y. Liu, Y. Cui, Nat. Nanotechnol. 12 (2017) 194–206.
[20] Y. Jiang, B. Wang, P. Liu, et al., Nano Energy 77 (2020) 105308.
[21] T. Li, X.Q. Zhang, P. Shi, Q. Zhang, Joule 3 (2019) 2647–2661.
[22] R. Xu, J.F. Ding, X.X. Ma, et al., Adv. Mater. 33 (2021) 2105962.
[23] J.F. Ding, R. Xu, X. Chen, et al., Angew. Chem. Int. Ed. 60 (2021) 11442–11447.
[24] J.F. Ding, R. Xu, C. Yan, et al., Chin. Chem. Lett. 31 (2020) 2339–2342.
[25] Y. Xu, H. Yan, T. Li, et al., Energy Storage Mater. 36 (2021) 108–114.
[26] J. Seok, N. Zhang, B. Ulgut, et al., Chem. Commun. 56 (2020) 11883–11886.
[27] B. Tong, J. Wang, Z. Liu, et al., J. Power Sources 400 (2018) 225–231.
[28] Y. Guo, P. Niu, Y. Liu, et al., Adv. Mater. 31 (2019) 1900342.
[29] C. Jin, O. Sheng, Y. Lu, et al., Nano Energy 45 (2018) 203–209.
[30] A. Pei, G. Zheng, F. Shi, Y. Li, Y. Cui, Nano Lett. 17 (2017) 1132–1139.